

You Can't See the Forest for Its Trees: Assessing Deep Neural Network Testing via NEURAL COVERAGE

Yuanyuan Yuan, Qi Pang, Shuai Wang
The Hong Kong University of Science and Technology
{yyuanaq, qpangaa, shuaiw}@cse.ust.hk

ABSTRACT

Recent works propose various deep neural network (DNN) coverage criteria to assess DNN test inputs and steer input mutations. Coverage is usually defined as the number of neurons whose outputs fall within certain ranges, and the range specifications distinguish these criteria. Despite the fact that a DNN is seen as a network of neurons with topological connections, its data and control flows are often constant when given diverse inputs. Observing the outputs of neurons alone is insufficient to define the behaviors of DNNs. As a result, recent research indicates that there is little correlation between the quality of test suites and neuron coverage criteria.

In general, DNNs approximate distributions, by incorporating hierarchical layers and neurons, in order to make decisions based on observed inputs. Thus, this work champions to deduce the behavior of a DNN from its approximate distributions. Accordingly, a test suite should be assessed from its induced neuron and layer output distributions. Meanwhile, to fully examine DNN behaviors, input mutation in typical DNN testing should be directed toward diversifying the approximated distributions.

This paper summarizes eight design requirements for DNN testing criteria, taking into account distribution properties and practical concerns. We then propose a new criterion, NLC, that satisfies all of these design requirements. NLC treats a single DNN layer as the basic computational unit (rather than a single neuron) and captures four critical features of neuron output distributions. Thus, NLC is denoted as NEURAL COVERAGE, which more accurately describes how neural networks comprehend inputs via approximated distributions rather than neurons. We demonstrate that NLC is significantly correlated with the diversity of a test suite across a number of tasks (classification and generation) and data formats (image and text). Its capacity to discover DNN prediction errors is promising. Test input mutation guided by NLC result in a greater quality and diversity of exposed erroneous behaviors.

1 INTRODUCTION

Recent work has incorporated software testing methodologies to successfully evaluate DNNs without the need for human annotations, for example, by transforming test inputs with always-hold relations (e.g., metamorphic relations) [51, 53, 59]. Such practice can effectively augment evaluation datasets and benchmark DNNs. However, fundamental understanding of a DNN's mechanism has remained largely unexplored due to its intrinsic non-linearity. Additionally, it has been observed that the decisions made by a DNN are susceptible to certain biases in the inputs [6, 15, 57]. As a result, DNN evaluation is highly dependent on the test suite's representativeness. Testing criteria is thus required to characterize a test

suite's quality and toward which the input mutations can comprehensively explore DNN behaviors.

In a manner similar to how coverage criteria are developed in traditional software testing, recent research proposes several neuron coverage criteria. In principle, the current criteria are mostly designed to monitor the outputs of neurons in a DNN model to assess the quality of test inputs. They argue that each neuron is an "individual computing unit" (as the authors put it [37]), or "individually encoding a feature" [31], comparable to a statement in traditional software. Further, despite that neuron outputs are continuous, existing criteria often first convert neuron outputs into discrete states (e.g., activation or not) to reduce the modeling complexity. Thus, by analyzing the discrete states of neurons, the DNN coverage exercised by an input is measured.

However, the key assumption — *each neuron is an individual computing unit* — often does not hold true for modern DNNs. Given a DNN is composed of stacked and non-linear blocks, the intermediate outputs (also known as latent representations) from neurons are continuous and highly entangled. Disentangling intermediate outputs remains a long-lasting challenge in the AI community [29, 30, 39]. And recent research in the software engineering community also points out that the efficacy of a test suite to uncover faults and existing neuron coverage attained by the test suite are not always positively correlated [17].

Establishing proper DNN coverage criteria requires a principled understanding about how DNN performs computations, which is fundamentally different with traditional software. A DNN, as a composition of parameterized non-linear functions (i.e., layers), extracts task-oriented features and then makes decisions accordingly. Features, hierarchically captured by layer outputs, approximate the posterior distribution of underlying explanatory factors H for observed inputs X , namely $P(H|X)$ [3, 4]. For example, given an image, layers in an image classifier extract hierarchical features that imply its class label [3]. More precisely, an image classifier generates a set of posterior distributions $P(h_i|x)$ (where i is the layer index, $h_i \in H$ and $x \in X$) with each h_i describes class-invariant properties of an image from different perspectives (e.g., shape, texture). The dependability of a DNN is defined as the degree to which the distribution, approximated on training data, is accurate when applied to real test data.

This work initializes a fresh and principled view on designing DNN coverage criteria, by assessing test inputs in terms of its induced neuron and layer output distributions. This work first concretizes our focus on distributions into eight design requirements of DNN testing criteria. These design requirements characterize the distribution approximated by a DNN from various perspectives, and also take practical constraints (e.g., speed, hyper-parameter free) into account. Then, we propose a new coverage criterion, namely

NLC (Neural Coverage), that can fully meet the design principles. NLC is referred to as “neural coverage” rather than neuron coverage since our study focuses on the overall activity of groups of neurons and consider relations of neurons, which distinguishes NLC from all existing efforts. Our evaluation encompasses nine DNNs that analyze a variety of data formats (e.g., image, text) and perform a variety of tasks (e.g., classification, generation). We demonstrate that NLC is substantially correlated with the diversity and capacity of a test suite to reveal DNN defects. Meanwhile, by taking NLC as the fuzzing feedback, we show that more and diverse errors can be found, and the error-triggering inputs mutated under the guidance of NLC manifest high naturalness. Our contributions are summarized as:

- This work advocates to design DNN testing criteria via a principled understanding about how DNN, with its hierarchical layers and neurons, approximate distributions. We argue that a proper DNN testing criterion should model the continuous neuron outputs and neuron entanglement in a comprehensive manner, instead of analyzing each neuron individually.
- We propose eight design requirements by characterizing the distributions approximated by a DNN and also taking into account practical implementation considerations. We accordingly design NLC, which satisfies all these requirements.
- We show that NLC can better assess the quality of test suites. NLC is particularly correlated with the diversity and fault-revealing capacity of a test suite. Fuzz testing under the guidance of NLC can also detect a large number of errors, which are shown as diverse and natural-looking.

2 PRELIMINARY

DNNs are often explained from the perspective of *distribution approximation* [3, 4, 45]. To motivate NLC, this section provides a high-level overview of DNNs from the distribution perspective.

Layer and Hierarchy. The term *network* in DNN refers to topological connections of non-linear layers. Each layer (e.g., a fully connected layer) has a group of neurons cooperating to process certain input features. The DNN *hierarchy* is established by gradually abstracting features from shallow to deep layers. For instance, image classifiers commonly collect shapes in an image at shallow layers and texture at deeper layers. Each layer (*not* each neuron) serves a minimal computing unit, whose output distribution encodes its focused features.

Neurons in a Layer. The term *neural* in DNN may be obscure. In cognitive science, neural signifies non-linear functions (e.g., Sigmoid) in DNNs that simulate how human neurons process signals [5, 42]. DNNs are powerful at analyzing high-dimensional media data and alleviating the curse of dimensionality due to their non-linearity [2, 3]. Moreover, outputs of neurons are *continuous*. Neurons in a layer are therefore highly *entangled*, impeding to comprehend the DNN’s internal mechanics.

Given a collection of data X labeled as Y , most popular DNNs can be categorized as discriminative and generative models, depending on how X and Y are involved in the *distribution approximation*.

Discriminative Models. Deep discriminative models approximate the conditional probability distribution $P(Y|X)$. A classification

model requires Y as discrete labels, and a regression model (e.g., forecasting) requires Y as a range of continuous values. For instance, a convolutional neural network (CNN) can classify images by extracting features (conveyed via outputs of intermediate neurons) and making decisions in one forward propagation. A layer outputs a conditional distribution denoting the extracted input features at this layer [3, 4, 45]. And with the extracted features getting more abstract at deeper layers, the ending layer returns the probability that the input belongs to each label. Sequential data, such as text, is typically processed by recurrent models, since the sequence, i.e., dependency between tokens, usually contains richer information. For example, an RNN conducting machine translation translates source language text into target language text. The model outputs one word every step, computing the conditional probability on all target words based on the current input word and processed words. **Generative Models.** Another popular paradigm is the deep generative model, which estimates the joint probability distribution $P(X, Y)$ of data X and label Y . The most common models are VAE [27] and GAN [16]. Generative models are primarily adopted to synthesize realistic data. To do so, both VAE and GAN project the data distribution to a simple distribution (e.g., normal distribution). To generate realistic outputs, random inputs sampled from the pre-defined distribution are fed into deep generative models.

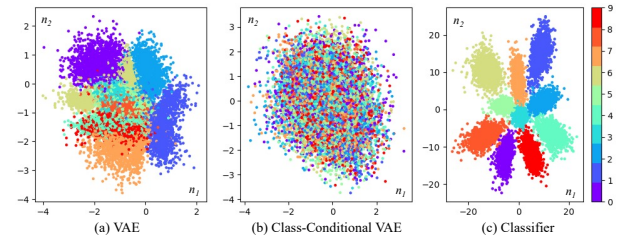


Figure 1: Visualization of n_1 and n_2 ’s outputs in three models extended from *Net*. X- and y-axis are outputs of n_1 and n_2 .

Visualizing DNN Outputs. We empirically assess and visualize distribution of intermediate neurons’ outputs. We prepare a DNN (denoted as *Net*) with two neurons n_1 and n_2 in the last layer (thus the dimensions are two) and extend *Net* into 1) a VAE, 2) a class-conditional VAE, and 3) a classifier model. The three models are trained on the MNIST dataset [11] for 1) random image generation, 2) labeled image (e.g., “2”) generation, and 3) image classification. In short, these three models inherent the same structure from *Net* yet perform different tasks by using different trailing layers. We plot outputs of n_1 and n_2 in these three models in Fig. 1.

Each dot denotes one output of n_1 and n_2 , corresponds to one image input. Multiple colors represent different labels of the inputs (e.g., red represents “9”). In Fig. 1(a), neuron outputs are jointly distributed corresponding to different labels. Fig. 1(c) shows a similar distribution, whereas the outputs are separated with labels to facilitate image classification. For Fig. 1(b), since class labels are provided as inputs, the model only captures common attributes of images. Therefore, outputs are not split.

This study examines the continuity of neuron outputs. Moreover, it considers neuron entanglement, where neurons in a layer jointly

form distributions that reflect how DNNs (of different tasks) understand input data distinctly. Also, outputs in high-density regions are not uniform. Rather, they tend to concentrate in the center.

NLC. Distributions formed by entangled neurons are important indicators of DNN behaviors. Given that “neural”, holistically, denotes the distributions of neuron outputs when understanding input features, this work proposes Neural Coverage, NLC, a new criterion that captures features in distributions formed in neuron outputs. The term “neural”, as an adjective, better reflects neuron outputs are processed in the continuous form and “L” also indicates each Layer is considered as the minimal computing unit.

3 MOTIVATION AND RELATED WORKS

This work proposes **eight requirements** to design a proper DNN testing criterion. We introduce the first three requirements in Sec. 3.1 and the rest five requirements in Sec. 3.2.

3.1 DNN Testing and Software Testing

Discrete vs. Continuous States. For software, coverage is typically measured by counting #statements, #basic blocks, or #paths executed by a test input. Accordingly, software testing aims to maximize code coverage, as high coverage suggests comprehensive testing. Inspired by software testing, previous DNN testing often first converts a neuron’s *continuous* outputs into two states, activated or not. Activation signals that a neuron is covered. Counting #activated neurons by a test input measures DNN coverage.

As shown in Fig. 1, a binary state (or a discretized state in general) is not expressive for describing neuron behavior. Instead, we advocate that a DNN coverage criterion should ① *precisely describe the continuous output of a neuron*.

Path vs. Layer. We argue that it is inaccurate to compare neurons to software statements. Each neuron is *not* as individual computing unit. In general, an “unactivated” neuron (in prior work’s [37] language) can still affect the subsequent neurons’ outputs and even the final output. Since DNN weights are fixed after training, contributions from each neuron are fixed (encoded in weights). However, software statements may not be covered regarding a particular input. On the other hand, Fig. 1 has shown that neuron outputs are often entangled to form joint distributions. Neuron entanglement is, to some extent, analogous to control-flow dependency, i.e., statements on the same path are executed together. Rather than studying individual neurons, it is preferable (and more efficient) to measure DNN coverage by ② *characterizing correlations of neurons*.

Execution vs. Estimation. Software executes its input on an execution path. DNNs, as described in Sec. 2, use a series of matrix and non-linear computations to approximate certain distributions given inputs as observations. Different DNN inputs produce different distributions, as seen in Fig. 1. Hence, further to ②, we advocate defining DNN criterion over the approximated distributions.

While it’s difficult to precisely describe the approximated distribution [38, 40, 55], certain informative properties of a distribution can be captured. Also, since coverage criteria are used to assess test suite quality and guide input mutations, knowing the exact distribution may not be required (see our empirical results in Sec. 7). In brief, we advocate that the DNN coverage criterion should analyze ③ *how outputs of neurons in a layer are distributed*.

3.2 Existing Neuron Coverage

We illustrate existing DNN coverage criteria in Fig. 2 using two neurons (in a layer) to ease reading. In general, existing coverage criteria discretize neuron outputs to decide if a neuron is “covered.” **Capturing “Major Behavior” of a Neuron.** The first criterion, namely neuron coverage (NC), was proposed in [37]. It is argued by [37] that the *major behavior* of a neuron is mostly reflected when its outputs are above zero. As in Fig. 2(a), NC deems a neuron as activated if its output is above threshold T (T is usually zero or a small value above). Following, three criteria were proposed [31], namely K-Multisection Neuron Coverage (KMNC), Neuron Boundary Coverage (NBC) and Strong Neuron Activation Coverage (SNAC). We display KMNC, NBC and SNAC in Fig. 2(b), Fig. 2(c) and Fig. 2(d). All three criteria first run training data to scope the output range of each neuron. Then, KMNC splits each range into K segments and regards coverage as #segments covered by neuron outputs. NBC denotes coverage as #neuron outputs lying outside the range, while SNAC counts coverage as #neurons whose outputs are larger than the upper bound of its normal value range. The intuition behind the three criteria is that the major behaviors of neurons are denoted as outputs that lie in the range decided by training data.

Considering the blue region in Fig. 1(c), it is easy to see that when feeding inputs of label “1”, NC over those two neurons will saturate. This indicates that criteria, which simply discretize neuron outputs, cannot properly describe the *diversity* of test suits (e.g., inputs of different labels). Moreover, note that all these criteria should not change if the **orange distribution** in Fig. 2(c) is rotated for 90 degrees (possibly due to fine-tuning). That is, these criteria might hardly reflect distinctly changed distributions of neuron outputs.

Further to ①, we argue that a neuron’s *major* behavior can hardly be defined using coarse-grained thresholds. Instead, given that the high-density regions formed by neuron outputs in a layer (the “dots” on the background of Fig. 2) are distinct on shapes, we deem the major behavior as the shapes which reflect the divergence of neuron outputs and the correlations among neurons. The corner-case behavior, accordingly, is regarded as neuron outputs lying in low-density regions. Therefore, we advocate that ④ *DNN coverage should take the density of neuron output distributions into account*. Holistically, measuring the density considers both major and corner-case behaviors of DNNs, which is desirable in software testing.

Discretizing Outputs of Several Neurons. Two layer-wise neuron coverage criteria were also proposed in [31], i.e., Top-K Neuron Coverage (TKNC) and Top-K Neuron Patterns (TKNP). Both criteria denote a neuron as activated if its outputs are ranked at top- K among neurons in a layer. TKNC counts #neurons once been activated, whereas TKNP records #patterns formed by activated neurons. In the case where there are two neurons in a layer, as we show in Fig. 2(e), a neuron is activated if its output is greater than the other one (i.e., $K = 1$ and $n_1 > n_2$). Despite considering all neurons in a layer, TKNC and TKNP are *not* able to comprehensively assess the diversity of a test suite, since both are easily saturated w.r.t. inputs of one or a few classes (see Fig. 1).

A cluster-based coverage (CC) was proposed in [36], in which the coverage is denoted as #clusters. Two clusters are formed if, the Euclidean distance of outputs from all neurons within a layer, is larger than a threshold. Given that the cluster is determined based

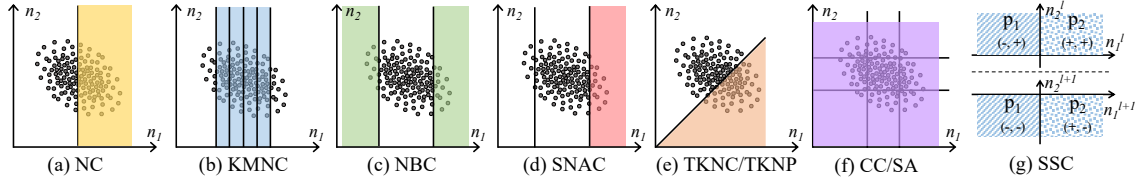


Figure 2: A schematic view of prior DNN coverage criteria. Two axes denote two neurons in a layer.

on distance, CC can be regarded as counting #regions formed by several neuron outputs as shown in Fig. 2(f). CC is more desirable than prior criteria given it is more comprehensive to overlay the joint distribution of neurons. Nevertheless, for the class-conditional VAE shown in Fig. 1(b), only inputs of one class can saturate CC, despite that inputs are far less being diverse. Also, CC could not capture correlations among neurons. Some recent studies propose coverage criteria based on the surprise adequacy (SA) [25, 26], which is a “distance” measure (in terms of neuron outputs) between a new input and historical inputs. More specifically, they discretize the distance range into several slots and count coverage as #slots covered by test suites. In that sense, they are conceptually variants of CC. See more details in Sec. **Comparison with Surprise Adequacy**.

The Sign-Sign Coverage (SSC) criterion was proposed in [48]. SSC captures the sign change of layer-wise adjacent neurons. A neuron is activated if 1) its outputs, and outputs from its adjacent neuron, have different signs for any pair of input $\langle p_1, p_2 \rangle$ (i.e., n_1^l and n_1^{l+1} in Fig. 2(g)) and simultaneously, 2) outputs from all other neurons with in the same layer have an identical sign for $\langle p_1, p_2 \rangle$ (i.e., n_2^l and n_2^{l+1} in Fig. 2(g)). SSC is specifically designed for ReLU-DNNs (i.e., DNNs with ReLU as the non-linear function). However, since most of the neuron outputs are nearly zero-centered due to input and layer normalization in modern DNNs [24, 47], SSC can be less useful for many of them. Also, while SSC takes the relation of adjacent layers into consideration, since each neuron is still a separate unit in SSC, the relation of layers is modeled in the neuron-level. As introduced in Sec. 2, the DNN hierarchy is formed by input feature re-use (e.g., processing object shape at shallow layers and then texture at deep layers). The hierarchy is generally encoded into layer outputs. NLC, by capturing the distribution of layer outputs, is more desirable compared to SSC.

Incorporating Training Data. The development of a DNN involves a “test-and-fix” procedure in which DNN is gradually fine-tuned to reduce its errors and fit on training data. This way, training data generally reflects DNN’s internal logic and property. We argue that ⑤ *DNN coverage should support incorporating prior-knowledge extracted from training data*. Existing criteria incorporate training data to scope neuron output ranges or to detect corner-case behaviors. Nevertheless, for some criteria, e.g., TKNC/TKNP, their hyper-parameter K depends on model structures instead of training data. NLC can incorporate training data to estimate distributions of neuron outputs before being used in online testing.

Implementation Considerations. DNN coverage criteria are often used in costly DNN testing. According to the released code of existing criteria, we notice that they are implemented in a *loop-fashion* which is slow. We find that testing frameworks guided by these criteria spend most (over 80%) of the time on coverage calculation. We re-implemented these criteria in a matrix-fashion, i.e.,

Table 1: Benchmarking coverage criteria for DNN testing. ✓, ◇, ✗ denote support, partially support, and not support.

	NC	KMNC	NBC	SNAC	TKNC	TKNP	CC	SSC	NLC
①	✗	✗	✗	✗	✗	✗	✗	✗	✓
②	✗	✗	✗	✗	◇	◇	✗	◇	✓
③	✗	✗	✗	✗	✗	✗	◇	✗	✓
④	✗	◇	✗	◇	✗	✗	✗	✗	✓
⑤	✓	✓	✓	✓	✗	✗	✓	✗	✓
⑥	✓	✓	✓	✓	✓	✓	✓	✗	✓
⑦	✓	✓	✓	✓	✓	✗	✗	✗	✓
⑧	✗	✗	✓	✓	✗	✗	✗	✓	✓

the calculation is performed as a sequence of matrix operations. Given that modern DL frameworks (e.g., PyTorch) can optimize matrix operations and also use hardware optimizations [9, 32, 43], the calculation is accelerated for over 100 times.

DNN coverage is often used to guide test input mutations. Since inputs are gradually fed, it is preferred if computing coverage incrementally. Ideally, given a new input, the cost for updating coverage should be roughly constant. Since TKNP iterates over existing patterns and #patterns increases when more data are produced, it does not support incremental computation. CC and SSC suffer from similar drawbacks. In sum, we advocate that ⑥ *a coverage criterion should support matrix-form computation to be optimizable by modern DL frameworks and hardware* and ⑦ *a coverage criterion should support incremental update*.

Most existing criteria rely on hyper-parameters. When using existing criteria, we find that coverage results are usually highly sensitive to hyper-parameters, whereas existing works hardly provide guidance to decide hyper-parameters under different scenarios. Viewing that deciding hyper-parameters likely requires expertise (in both software testing and deep learning), we advocate that ⑧ *a DNN coverage is desirable to be hyper-parameter free*.

Comparison with Existing Criteria. Table 1 benchmarks existing DNN coverage criteria (and NLC) w.r.t. the eight requirements summarized in this section. Note that TKNC/TKNP considers the relative relation of neuron outputs and SSC considers the sign relation between two neurons. They are deemed as partially satisfying ②. Similarly, since CC counts #regions formed by several neurons, it partially fulfills ③. Also, given that neuron outputs concentrate on center points, the neuron output range overlays the high-density regions. We thus regard KMNC, NBC and SNAC as partially satisfying ④. In contrast, we emphasize that NLC can satisfy all these requirements, as will be introduced in Sec. 4.

4 DESIGN OF NLC

As mentioned in Sec. 3.1, it’s generally difficult to precisely and efficiently describe distributions approximated by DNNs [38, 40, 55].

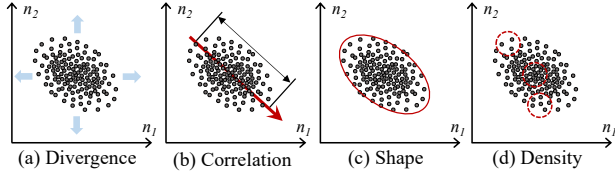


Figure 3: Four properties describing neuron output distributions. We take these properties into account to form NLC.

Instead, NLC captures four key properties of distributions, namely the divergence, correlation, shape, and density, as depicted in Fig. 3. In Sec. 7, we present empirical results to show that these properties are sufficient to constitute a criterion that outperforms all existing works. We now elaborate on each property in details.

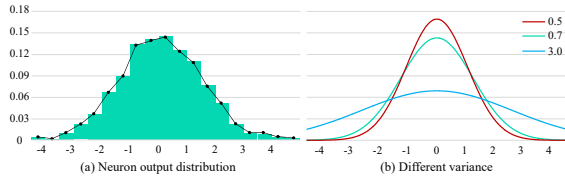


Figure 4: Output distribution of one neuron from ResNet50.

Measuring Activation in Continuous Space. Neuron outputs are continuous floating-point numbers. Instead of discretizing their continuous outputs, we directly measure them in the continuous space. We start with the case of one neuron.

We randomly select one neuron from a pretrained ResNet50 and plot its output distribution in Fig. 4(a) using all images in its training dataset. The x-axis denotes the output value and the y-axis denotes the ratio of involved inputs. Consistent with Fig. 1, output values converge to a certain point (zero in this case). NLC directly measures how divergent (i.e., the activation) the neuron output is in its continuous form by calculating the following variance:

$$\sigma_n^2 = \mathbb{E}[(n - \mathbb{E}[n])(n - \mathbb{E}[n])], \quad (1)$$

where n is the output of a neuron. Overall, variance is widely-adopted for characterizing the divergence of a collection of samples. Eq. 1 increases when output values spread along the x-axis. In contrast, if most outputs are zero, the variance will decrease, as in Fig. 4(b). Variance serves as an important descriptor of neuron output distributions. A test suite is regarded as comprehensive if it results in a high variance. Similarly, input mutations can be launched towards the direction that increases variance. Comparing with previous criteria, we require no discretization, thus taking all distinct neuron outputs into account (in response to ①). In addition, Eq. 1 does not ship with hyper-parameters (respond to ⑧).

Characterizing Neuron Entanglement. As noted in Sec. 2, neurons in a layer are entangled and jointly process input features. As empirically assessed in Fig. 1, neurons manifest distinct correlations under different tasks and for inputs of different classes. For example, in Fig. 1(c), one neuron is positively (e.g., class “1”) or negatively (e.g., class “9”) correlated with the other neuron.

Fig. 5 presents three different correlations of two neurons, namely, no correlation, positive correlation and negative correlation. Given

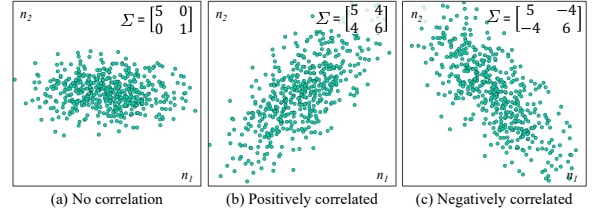


Figure 5: Neurons having various correlations.

that there are more than one neuron, the DNN coverage should simultaneously consider the divergence of each neuron and correlations among neurons. Eq. 1 uses variance to describe divergence of a neuron’s output, i.e., $\sigma_{n_1}^2$ and $\sigma_{n_2}^2$. Similarly, we use the covariance, a common metric for joint variability of two variables, to characterize the correlation between two neurons. Thus, the correlation between the two neurons is formulated as

$$\varsigma_{n_1, n_2} = \mathbb{E}[(n_1 - \mathbb{E}[n_1])(n_2 - \mathbb{E}[n_2])] = \varsigma_{n_2, n_1}. \quad (2)$$

$\varsigma_{n_1, n_2} = 0$ implies that n_1 and n_2 are not correlated, whereas $\varsigma_{n_1, n_2} > 0$ denotes a positive correlation between n_1 and n_2 , i.e., n_1 will increase with n_2 , and vice versa. A higher ς_{n_1, n_2} denotes a stronger correlation. The same holds when $\varsigma_{n_1, n_2} < 0$. Taking Eq. 1 and Eq. 2 into account, we simultaneously represent the divergence of each neuron and correlations of neurons in a unified form as

$$\Sigma = \begin{bmatrix} \sigma_{n_1}^2 & \varsigma_{n_1, n_2} \\ \varsigma_{n_2, n_1} & \sigma_{n_2}^2 \end{bmatrix}, \quad (3)$$

where Σ is the covariance matrix of n_1 and n_2 . As we show in Fig. 5, the value of ς_{n_1, n_2} also represents the divergence along the “correlation direction” of two neurons. Thus, we use

$$\frac{1}{m \times m} \|\Sigma\|_1 = \frac{1}{m \times m} \sum_{j=1}^m \left(\sum_{i=1}^m |\varsigma_{n_i, n_j}| \right), \quad (4)$$

where m is #neurons and $\varsigma_{n_i, n_i} = \sigma_{n_i}^2$, to represent the DNN coverage. The size of Σ is $m \times m$ and $\frac{1}{m \times m}$ works as the normalization term to eliminate the affect of #neurons to the coverage values. In the case where more than two neurons are correlated, e.g., n_i , n_j and n_k , Σ will characterize the entanglement via ς_{n_i, n_j} , ς_{n_i, n_k} and ς_{n_j, n_k} . Hence, Eq. 4 facilitates addressing requirements ① and ②. Note that Σ can be set using the correlation term ς_{n_i, n_i} decided by training data. Therefore, it conceptually subsumes the neuron output range leveraged by KMNC to recognize major DNN behaviors. The key difference is that Σ denotes major behaviors as the majority of neuron correlations (i.e., the shape of the distribution). Also, Σ can be further refined in a class conditional manner by extending the size to $c \times m \times m$ where c is #classes. It thus will be calculated by first indexed using the class labels. In both two cases, NLC fulfills the requirement of ⑤.

We note that NLC employs Eq. 4 over all neurons in each layer. Thus, ③, which champions modeling the distribution of neuron outputs in a layer, is taken into account. Further, given a DNN contains multiple layers, the coverage of DNN is computed as

$$\text{NLC} = \sum_l \frac{1}{m^l \times m^l} \|\Sigma^l\|_1, \quad (5)$$

where l is the layer index. A higher NLC indicates a more diverse test suite. Test input mutations, accordingly, are expected to accumulate towards directions that maximize NLC.

Capturing Distribution Shape. Unlike previous works where each neuron is considered separately, we take neurons from the same layer as a group. As in Fig. 1, the output distribution of neurons in the same layer is mostly distinct under different tasks. Moreover, for the separated regions (in different colors) under certain tasks (e.g., classification), they may also have different shapes characterizing various DNN behaviors. Hence, we capture a major behavior by describing the shape of a distribution. We now explain why Σ in Eq. 3 captures a distribution’s shape.

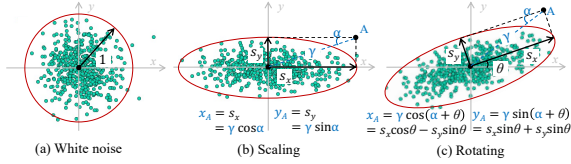


Figure 6: Transforming white noise to a desired distribution.

To ease the understanding, we first show how to transform a white noise (whose covariance matrix is degenerated into an identity matrix I) to the distribution formed by outputs from a group of neurons. Fig. 6(a) displays a white noise \mathcal{N} and Fig. 6(c) presents the output distribution of two neurons, namely x and y . Thus, the transformation can be decomposed into two elementary operators – scaling and rotating. The scaling operator spreads the two neuron outputs and the rotating operator introduces correlations between x and y . The rotating and scaling operations are defined by rotation matrix and scaling matrix as

$$\mathcal{R}_{2 \times 2} = \begin{bmatrix} \cos \theta & -\sin \theta \\ \sin \theta & \cos \theta \end{bmatrix}, \mathcal{S}_{2 \times 2} = \begin{bmatrix} s_x & 0 \\ 0 & s_y \end{bmatrix}, \quad (6)$$

respectively. Thus, the output distribution can be represented as $(\mathcal{R}\mathcal{S})\mathcal{N}$. Following Eq. 1 and Eq. 2, we have

$$\begin{aligned} \Sigma &= \mathbb{E}[(\mathcal{R}\mathcal{S}\mathcal{N} - \mathbb{E}[\mathcal{R}\mathcal{S}\mathcal{N}])(\mathcal{R}\mathcal{S}\mathcal{N} - \mathbb{E}[\mathcal{R}\mathcal{S}\mathcal{N}])^\top] \\ &= (\mathcal{R}\mathcal{S})\mathbb{E}[(\mathcal{N} - \mathbb{E}[\mathcal{N}])(\mathcal{N} - \mathbb{E}[\mathcal{N}])^\top](\mathcal{R}\mathcal{S})^\top \\ &= (\mathcal{R}\mathcal{S})I(\mathcal{R}\mathcal{S})^\top = (\mathcal{R}\mathcal{S})(\mathcal{R}\mathcal{S})^\top, \end{aligned} \quad (7)$$

which indicates that covariance matrix Σ in Eq. 3 encodes transformations from a white noise to a desired distribution. Therefore, we illustrate that the covariance matrix captures the shape of the output distribution formed by outputs of neurons in a layer.

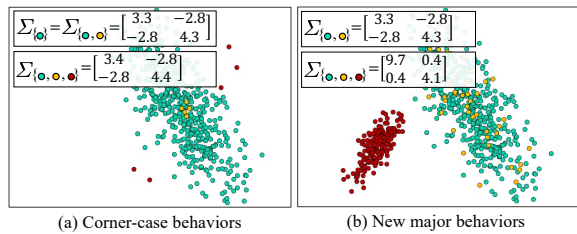


Figure 7: Density.

Responding to Local Density Change. Neuron outputs generally concentrate to certain points to form clusters, and the density

varies in the output space. We first elaborate on what may introduce a local density change. Recall that we deem corner-case behaviors as neuron outputs lying at the low-density regions (e.g., boundary of one cluster), which are likely to trigger DNN defects. Given that these outliers typically have much lower local-density, their existence will lead to density change. Previous works (e.g., NBC, SNAC) characterize the corner-case behavior as out-of-range outputs of a neuron. Since neuron outputs will gather at multiple regions for certain tasks, some rare outputs (i.e., the corner cases) still lie in the range decided by the majority of neuron outputs. Consider Fig. 7(a) where the DNN outputs in red are deemed as outliers. Nevertheless, since they are still in the output ranges formed by all green dots, SNAC and NBC will not treat them as corner case behaviors. In fact, the new red outputs will *not* induce coverage increase for all previous criteria except CC, since CC divides the entire output space into grids. However, CC requires a properly selected grid size, which is a hyper-parameter configured by users.

Also, for certain cases where neuron outputs are separated (e.g., the classifier in Fig. 1(c)), the appearance of a new major behavior (e.g., images get classified as a new class) also leads to density change. As shown in Fig. 7(b), the newly-formed cluster of red dots denotes a new major behavior of the DNN, nevertheless, NC possibly has no response since their values are lower than the threshold.

We show that NLC responds to density change. For Fig. 7(a), the $\|\Sigma\|_1$ of existing green dots is 13.2. It will be updated as 13.4 given the new red dots, which will lead to a response to our criterion. Whereas for the new yellow dots, since it stays close to the majority of existing outputs, our criterion has no response. Meanwhile, for Fig. 7(b), the $\|\Sigma\|_1$ will change from 13.2 to 14.6 when the cluster formed by red dots appears. We thus state that our criterion can respond to density change which is possibly introduced by corner-case behaviors and new major behaviors. This way, NLC satisfies ④, which requires DNN coverage to take the density of neuron outputs into account.

5 IMPLEMENTATION CONSIDERATIONS

From Sec. 4, it is easy to see that NLC supports matrix-form computing and has no hyper-parameters. Thus, NLC satisfies ⑥ and ⑧. We now clarify that NLC also satisfies the requirement of incremental computing (requirement ⑦). We also show that NLC supports batch computation, which is also vital as DNNs generally take a batch of inputs and the batch size varies from 1 to hundreds. Let existing data be \mathbb{B} , given a batch of new data B , the covariance matrix Σ (Eq. 4) of each layer can be calculated as

$$\begin{aligned} \Sigma &= \frac{|\mathbb{B}| \times |B| \times (\mu_{\mathbb{B}} - \mu_B)(\mu_{\mathbb{B}} - \mu_B)^\top}{(|\mathbb{B}| + |B|)^2} \\ &+ \frac{|\mathbb{B}| \times \Sigma_{\mathbb{B}} + |B| \times \Sigma_B}{|\mathbb{B}| + |B|}, \end{aligned} \quad (8)$$

where μ represents the mean of a collection of data. It is clear to see that Eq. 8 does *not* iterate over existing data and update Σ incrementally. Accordingly, NLC formed in Eq. 5 satisfies ⑦.

COMPARISON WITH SURPRISE ADEQUACY

Three Surprise Adequacy (SA) [25, 26], namely, Likelihood-based SA (LSA), Distance-based SA (DSA) and Mahalanobis Distance-based SA (MDSA) are proposed in previous works. All SAs measure the interest for a new input based on its dissimilarity, which is a real value and can be regarded as a *distance*, to historical inputs in terms of neuron outputs. Several coverage criteria can be derived from SAs, in general, they first divided the range of “distance” into slots and then count coverage as #covered slots. Conceptually, they can be regarded as variants of CC since each distance-slot can be viewed as a cluster and the threshold deciding new cluster is the slot size. The difference is how to calculate the “distance”: CC employs Euclidean distance but SA-based coverage criteria use SAs.

LSA characterizes the dissimilarity using density estimated by Gaussian kernel function: a new input is more desired if it appears in a low-density region. Note that a cluster is defined as a high-density region and a point introduces a new cluster when it lies in a low-density region. That is, when solely adopting LSA to measure the dissimilarity for a DNN input (e.g., a lower density value), it is equivalent to prioritize inputs using CC (e.g., a higher CC value). Also, despite LSA considers multiple neurons, it does not reflect neuron correlation and treats neurons independently. LSA excludes neurons with low output-variances; nevertheless, a lower variance of neuron outputs does not necessarily indicate less significance, as a smaller output range also induces lower variance. In fact, this is common since modern DNNs use normalization layers to normalize neuron outputs around zero. Moreover, given that modern DNNs have millions of neurons, the kernel density estimation in LSA is infeasible for such extremely high-dimension variable.

For implementation consideration, both LSA and DAS do not support incremental update (i.e., ⑦) and LSA has hyper-parameters which violates ⑧. We note that both MDSA and NLC adopt covariance. However, we clarify that the two “covariance” are used in distinct aspects. NLC characterizes how fresh inputs change the neuron relation, or lead to a new distribution, using an actively-updated covariance. NLC incrementally updates covariance given new inputs and rollbacks the value if new input is not desired. Nevertheless, the covariance in MDSA does not describe how neuron relation, or distribution, change given new inputs. It is a pre-computed constant which, together with the output mean, represents the distribution of historical neuron outputs, such that Mahalanobis distance can be computed. We point out that the intuition behind Mahalanobis distance assumes that historical neuron outputs follow a Gaussian distribution, which is impractical given that neuron output distribution is intractable and estimating this distribution is still an open problem.

6 EVALUATION SETUP

NLC is implemented using PyTorch (ver. 1.9.0) with roughly 2,300 LOC. All experiments are launched on one Intel Xeon CPU E5-2683 with 256GB RAM and one Nvidia GeForce RTX 2080 GPU. We will introduce all target DNNs and datasets along with each launched experiment in Sec. 7. We now introduce detailed settings of DNN coverage criteria compared with NLC.

Table 2: DNN Models used in Sec. 7.1. All image models are trained on CIFAR10 and ImageNet.

Model	#Neuron	#Layer	Remark
ResNet50 [18]	26,570/27,560	54	Non-sequential topology
VGG16_BN* [46]	12,426/13,416	16	Sequential topology
MobileNet-V2 [23]	17,066/18,056	53	Mobile devices
BigGAN [7]	6,403/48,627	11/41	Generative model
LSTM [22]	32,769	129	Text model

*All image models have batch normalization (BN) layers.

Table 3: Datasets (train/test) used in Sec. 7.1. Each class has the same number of images.

Dataset	CIFAR10	ImageNet	IMDB
#Classes	10	100	2
#Data	50,000/10,000	100,000/5,000	17,500/17,500

Neuron Coverage (NC). The authors of NC state that a neuron is “activated” if its output is higher than a threshold T [37]. Some previous works [31] also evaluate NC following this setting. However, according to the official codebase of NC [1], they first rescale all neuron outputs in a layer to $[0, 1]$ and the activation of one neuron is decided on the rescaled value. We also implement this variant of NC (referred to as NCS). NC is evaluated given $T \in \{0, 0.3, 0.6\}$ and for NCS, $T \in \{0.25, 0.5, 0.75\}$.

K-Multisection Neuron Coverage (KMNC). KMNC has one hyper-parameter K noting the #segments for a neuron output. We choose K in $\{10, 100, 1000\}$.

Top-K Neuron Coverage/Patterns (TKNC/TKNP). TKNC and TKNP monitor neurons with top- K highest outputs among neurons in a layer. We configure $K \in \{1, 10, 100\}$.

Cluster-based Coverage (CC). CC denotes two layer-outputs as lying in two clusters if their Euclidean distance is larger than a threshold T . T primarily depends on specific DNNs. We introduce T in each experiment.

SSC is specifically designed for ReLU-DNN, whereas modern DNNs have various non-linear functions. Also, SSC does *not* support matrix-form and incremental computing. Our preliminary study shows that due to a large number of neurons in modern DNNs, SSC is not applicable (too slow). We thus omit to compare with it.

7 EVALUATION

7.1 Assessing Test Suite Quality

We first compare NLC with existing criteria on its effectiveness to 1) assess the diversity of test suites and 2) characterize the fault-revealing capability of test suites.

Settings. We evaluate NLC on both discriminative and generative models. The involved models and datasets are listed in Table 2 and Table 3. For discriminative models, we choose VGG16, ResNet50, and MobileNetV2, which represent popular models on mobile platforms and standard large-scale DNNs with sequential and non-sequential topological structures. The three models are trained on two datasets of different scales, namely, CIFAR10 [28] and ImageNet [10]. Models trained on CIFAR10 have over 92% test accuracy and those trained on ImageNet are provided by PyTorch. CIFAR10 is composed of 32×32 images labeled as ten classes. ImageNet contains images of 1,000 classes and the average image size is 469×387 . To speed up the progress, we randomly select 100

classes from ImageNet. We also evaluate NLC on the text model, i.e., a LSTM [22] trained on the IMDB dataset [34] for sentiment analysis [14]. Given that each layer in the LSTM is unrolled to process sequential inputs, the unrolled layers are deemed separate for computing coverage. For generative models, we choose the SOTA model BigGAN. The BigGAN is also trained on CIFAR10 and ImageNet.

Diversity. To assess the diversity of test suites for discriminative models, we construct two datasets of different diversity using schemes noted as $\times 1$ and $\times 10$. For the $\times 1$ scheme, we randomly choose 100 images from the test data and add white noise to produce mutated images (the total number of mutated images in $\text{test}_{\times 1}$ equals to the size of test). The white noise is truncated within $[-0.1, 0.1]$ to preserve the appearance of images. Given that text is discrete, it is infeasible to add white noise. We thus randomly shuffle words in the 100 selected sentences to produce meaningless sentences. The $\times 10$ scheme follows the same procedure, but the number of the produced data is 10 times of the test data. The diversity of these datasets (**ground truth** of Table 4 and Table 5) are ranked as $\text{test} > \text{test}_{\times 10} > \text{test}_{\times 1}$, because test contains over 10K diverse images in real-world datasets, whereas $\text{test}_{\times 10}$ and $\text{test}_{\times 1}$ are generated by (slightly) mutating 100 real images.

For the generative model, it generates images by sampling from a fixed distribution (i.e., the normal distribution). Since the generation procedure is conditioned on a given class label, we construct datasets of different diversity by following the *Normal*, N/x and C/x schemes (see Table 6). For the *Normal* scheme, we sample total m inputs from the normal distribution and each class has the same number of inputs. For the N/x scheme, we only keep $1/x$ of inputs from each class, whereas for the C/x scheme, we only keep $1/x$ of classes. We set m to 32,000 and choose $x \in \{2, 10\}$. Since inputs conditioned on different classes are all sampled from normal distribution, behaviors of generative models are primarily decided by the class labels. Thus, the diversity of these datasets (**ground truth** of Table 6) are ranked as: *Normal* $>$ $N/2 > N/10 > C/2 > C/10$.

Given that each model is deployed using the training data, we show the increased coverage of the corresponding test data and its variants in Table 4, Table 5 and Table 6 for image models, text models, and generative models, respectively. All experiments are launched for five times to reduce randomness.

Existing criteria (except for NBC and SNAC) require extra hyper-parameters, and their evaluation results are largely determined by these hyper-parameters. For instance, all variants of CIFAR10 test data have zero coverage when T of NC is 0.6, whereas they reach a saturation coverage when K of TKNP is 10 (i.e., #patterns equals to #inputs) despite they are still evaluated on same models. Moreover, the hyper-parameter T of CC is model specific, for instance, $T = 10$ is suitable for ResNet trained on CIFAR10, but is too small if the ResNet is trained on ImageNet — any input will form a new cluster. We thus increase T 100 times for models trained on ImageNet. Again, without prior knowledge on setting hyper-parameters, it is obscure to adopt these criteria in real-life usage. In contrast, NLC is hyper-parameter free, enabling an “out-of-the-box” usage.

For most cases of image models and text models, the $\times 1$ scheme and the test dataset have comparable results, and the $\times 10$ scheme

Table 4: Coverage achieved by different datasets on image models. CR and IN denote CIFAR10 and ImageNet. Assessments matching ground truth are marked .

Criteria	Config.	DNN	CR	CR $\times 1$	CR $\times 10$	IN	IN $\times 1$	IN $\times 10$
NC (%)	$T=0$	ResNet	0.037	0.030	0.113	0.025	0.022	0.028
		VGG	0.096	0.145	0.177	0.007	0.007	0.015
		MobileNet	0.046	0.058	0.094	0	0	0.005
	$T=0.3$	ResNet	0	0	0	0.036	0.018	0.037
		VGG	0.58	0.33	0.63	0	0	0.045
		MobileNet	0	0	0	0.016	0.022	0.038
	$T=0.6$	ResNet	0	0	0	0	0	0.004
		VGG	0	0	0	0	0	0.002
		MobileNet	0	0	0	0.044	0.027	0.078
NCS (%)	$T=0.25$	ResNet	0.026	0.031	0.031	0	0	0
		VGG	0.113	0.177	0.225	0	0	0
		MobileNet	0	0	0	0	0	0
	$T=0.5$	ResNet	0.75	1.14	2.10	0	0	0.01
		VGG	0.56	0.77	1.09	0	0	0.01
		MobileNet	0.02	0.01	0.05	0	0	0
	$T=0.75$	ResNet	2.15	2.52	4.54	0.13	0.21	0.38
		VGG	2.49	3.25	4.27	0.02	0	0.02
		MobileNet	1.57	1.69	2.17	0.02	0.02	0.03
KMNC (%)	$K=10$	ResNet	8.89	40.01	40.50	4.10	4.25	5.59
		VGG	7.33	55.25	55.50	4.19	8.34	9.17
		MobileNet	8.53	8.97	10.43	4.67	4.52	6.82
	$K=100$	ResNet	8.52	26.96	28.37	2.17	5.08	5.14
		VGG	7.54	45.25	45.60	1.36	5.22	5.26
		MobileNet	4.81	10.02	10.19	1.43	2.15	3.01
	$K=1,000$	ResNet	3.99	10.64	10.78	1.87	4.29	4.31
		VGG	2.84	12.36	12.50	0.91	2.61	2.68
		MobileNet	4.61	8.38	8.69	2.01	3.44	3.92
NBC (%)	N/A	ResNet	0	1.75	4.85	0.13	0.48	1.20
		VGG	0.27	2.04	2.12	0.08	0.13	0.23
		MobileNet	0.003	2.46	2.51	0.15	0.20	0.32
SNAC (%)	N/A	ResNet	0	0.97	2.62	0.14	0.57	0.73
		VGG	0.53	1.52	1.64	0.13	0.01	0.23
		MobileNet	0	1.41	2.37	0.15	0.27	0.38
TKNC (%)	$K=1$	ResNet	0.20	0.23	0.41	0.06	0.03	0.10
		VGG	0.81	1.20	1.97	0.29	0.13	0.44
		MobileNet	0.24	0.13	0.28	0.10	0.06	0.20
	$K=10$	ResNet	0.38	0.36	0.68	0.11	0.02	0.14
		VGG	2.29	2.66	3.83	0.01	0.01	0.01
		MobileNet	0.21	0.12	0.31	0.03	0.03	0.03
	$K=50$	ResNet	0.24	0.23	0.45	0.03	0.01	0.06
		VGG	3.07	3.35	4.57	0.01	0.02	0.02
		MobileNet	0.17	0.22	0.38	0.02	0	0.05
TKNP (#)	$K=1$	ResNet	9,995	9,586	80,561	4,900	3,954	23,384
		VGG	6,060	6,809	36,887	4,882	3,386	17,187
		MobileNet	9,998	9,924	90,537	4,900	5,000	48,083
	$K=10$	ResNet	10,000	10,000	100,000	4,901	5,000	50,000
		VGG	10,000	10,000	100,000	4,901	5,000	50,000
		MobileNet	10,000	10,000	100,000	4,901	5,000	50,000
	$K=50$	ResNet	1,034	434	1,823	4,901	5,000	50,000
		VGG	10,000	10,000	100,000	4,901	5,000	50,000
		MobileNet	694	650	1,665	4,901	5,000	50,000
CC* (#)	$T=10$ $T=1,000$	ResNet	55	44	60	4,945	1,333	9,787
		VGG	147	137	168	14,532	2,148	7,681
		MobileNet	37	29	38	4,947	4,614	43,613
	$T=20$ $T=2,000$	ResNet	19	19	23	4,918	397	9,771
		VGG	51	48	63	11,914	954	1,606
		MobileNet	9	10	11	4,946	2,618	12,466
	$T=50$ $T=5,000$	ResNet	9	7	9	4,130	256	8,263
		VGG	22	21	22	4,526	426	571
		MobileNet	7	4	7	4,943	346	531
NLC	N/A	ResNet	1.03	0.05	0.47	6006.38	11.00	113.37
		VGG	403.95	0	0	20327.50	49.50	413.50
		MobileNet	0.61	0.12	0.23	10693.50	86.25	757.25

* $d \in \{10, 20, 50\}$ for models trained on CIFAR10 and $d \in \{1000, 2000, 5000\}$ for models trained on ImageNet.

has the highest coverage. Given datasets created by $\times 1$ have identical size with the test dataset, we interpret that existing neuron coverage criteria are more sensitive to the *number* of data samples rather than the diversity. Nevertheless, the coverage assessed by NLC are consistent with the diversity of these datasets (i.e., the

Table 5: Coverage achieved by different datasets on text models. Assessments matching ground truth are marked .

Criteria	Config.	DNN	IMDB	IMDB _{x1}	IMDB _{x10}
NC (%)	T=0	LSTM	1.25	2.32	2.41
	T=0.3	LSTM	0.42	0.87	1.52
	T=0.6	LSTM	0.17	0.41	0.72
NCS (%)	T=0.25	LSTM	0.012	0.018	0.034
	T=0.50	LSTM	0.015	0.018	0.027
	T=0.75	LSTM	2.191	1.001	2.554
KMNC (%)	K=10	LSTM	7.68	3.69	12.11
	K=100	LSTM	1.92	2.99	5.31
	K=1,000	LSTM	0.05	0.08	0.15
NBC	N/A	LSTM	0.12	0.04	0.13
SNAC	N/A	LSTM	0.11	0.03	0.03
TKNC (%)	K=1	LSTM	0.28	0.19	0.67
	K=10	LSTM	0.50	0.39	0.96
	K=50	LSTM	1.34	1.20	2.86
TKNP (#)	K=1	LSTM	20,252	12,118	101,789
	K=10	LSTM	6,515	2,224	8,602
	K=50	LSTM	11,830	4,633	20,479
CC (#)	T=10	LSTM	266	265	283
	T=20	LSTM	134	137	146
	T=50	LSTM	57	1	65
NLC	N/A	LSTM	1279.81	11.01	132.99

ground truth). Moreover, despite the number of $\times 10$ variant is 10 times of test data, its reflected coverage on NLC is smaller, which indicates that NLC successfully reflects the diversity of the inputs.

For generative models like BigGAN, inputs for both training and test phases are random variables sampled from the normal distribution. Infinite “training data” exists, and therefore, KMNC, NBC and SNAC are infeasible to use, as they assign each neuron an output range decided by the training data. In practice, we find that coverage measured by them tend to be random. In contrast, NLC, by default, can be used with no training data, and it can be adopted in both discriminative and generative models. For the remaining coverage criteria, most of their results are ranked as $Normal > N/2 > C/2 > N/10 > C/10$, which further reflects that prior criteria are more sensitive to the number of inputs instead of their diversity. Since previous criteria analyze neuron outputs separately, feeding more inputs might possibly increase the chance of activating more neurons in a linear manner. In contrast, NLC analyzes the formed distributions among neurons, where most “trivial” inputs will not influence the correlations or distributions. In contrast, since a diverse test suite possibly uncovers different correlations among neurons, NLC becomes more responsible for a diverse test suite.

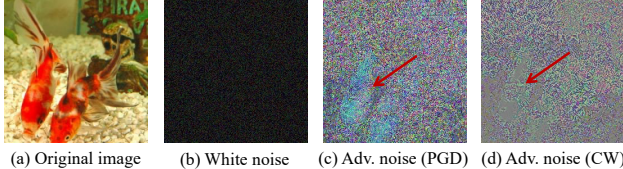


Figure 8: Adversarial perturbations.

Fault-Revealing Capability. To evaluate the fault-revealing capabilities of test suites, we construct adversarial examples (AE) using

Table 6: Coverage achieved by different datasets on generative models. BigGAN_C and BigGAN_I refer to BigGAN trained on CIFAR10 and ImageNet. Assessments matching ground truth are marked .

Criteria	Config.	DNN	Normal	N/2	N/10	C/2	C/10
NC	T=0	BigGAN _C	97.19	96.89	96.31	96.56	94.45
		BigGAN _I	85.88	85.65	85.05	85.56	84.59
	T=0.3	BigGAN _C	59.21	55.61	44.90	54.41	40.76
		BigGAN _I	14.41	13.82	12.03	12.96	10.47
	T=0.6	BigGAN _C	16.40	15.40	13.62	14.12	9.68
		BigGAN _I	6.92	6.56	5.50	6.07	5.14
NCS	T=0.25	BigGAN _C	99.97	99.97	99.95	99.97	99.95
		BigGAN _I	99.43	99.42	99.40	99.42	99.39
	T=0.5	BigGAN _C	99.34	99.30	99.02	99.25	98.73
		BigGAN _I	94.18	93.96	93.44	93.87	93.44
	T=0.75	BigGAN _C	86.66	84.88	79.70	82.85	76.90
		BigGAN _I	81.64	81.30	80.17	80.98	77.61
KMNC	K=10	BigGAN _C	54.72	56.00	54.71	54.24	52.44
		BigGAN _I	58.15	57.06	58.14	56.20	56.82
	K=100	BigGAN _C	21.54	21.45	21.84	21.83	21.48
		BigGAN _I	22.66	22.33	22.59	22.20	22.32
	K=1000	BigGAN _C	3.04	3.04	3.04	3.04	3.03
		BigGAN _I	3.07	3.08	3.07	3.07	3.06
NBC	N/A	BigGAN _C	0.22	0.09	0.04	0.09	0.10
		BigGAN _I	0.54	0.21	0.21	0.03	0.06
SNAC	N/A	BigGAN _C	0.02	0.03	0.03	0.03	0.03
		BigGAN _I	0.03	0.07	0.04	0.64	0.14
TKNC	K=1	BigGAN _C	31.69	27.75	16.95	27.16	15.56
		BigGAN _I	16.79	14.56	9.62	13.11	5.91
	K=10	BigGAN _C	62.64	58.89	48.34	58.46	45.14
		BigGAN _I	34.92	33.77	29.90	32.44	22.62
	K=50	BigGAN _C	83.96	81.45	75.03	81.23	73.54
		BigGAN _I	42.02	41.68	40.58	41.27	38.08
TKNP	K=1	BigGAN _C	31,415	15,843	3,193	15,779	3,134
		BigGAN _I	32,000	16,000	3,200	16,000	3,200
	K=10	BigGAN _C	32,000	16,000	3,200	16,000	3,200
		BigGAN _I	32,000	16,000	3,200	16,000	3,200
	K=50	BigGAN _C	32,000	16,000	3,200	16,000	3,200
		BigGAN _I	10,894	6,898	2,088	6,997	2,178
CC	T=50	BigGAN _C	347	302	175	232	89
		BigGAN _I	1,204	921	485	780	324
	T=100	BigGAN _C	90	70	40	50	18
		BigGAN _I	323	266	147	239	108
	T=200	BigGAN _C	27	25	13	23	7
		BigGAN _I	105	99	77	95	64
NLC	N/A	BigGAN _C	1051.63	776.29	653.62	280.67	178.92
		BigGAN _I	3596.89	3306.88	3141.02	2636.64	1462.11

Table 7: Coverage achieved by test data and AEs of CIFAR10. Assessments matching ground truth are marked .

	Data	NC T=0 (%)	NCS T=0.75 (%)	KMNC K=100 (%)	NBC (%)	SNAC (%)	TKNC K=10 (%)	TKNP K=50 (#)	CC T=10 (#)	NLC
ResNet	Test	0.04	2.15	8.52	0	0	0.38	1,034	55	1.03
	CW	0.11	0.90	0	3.94	2.73	0.18	31	5	2.44
	PGD	0.24	1.43	0	13.83	23.22	0.35	680	29	22.92
VGG	Test	0.10	2.49	7.54	0.27	0.53	2.29	10,000	147	403.95
	CW	0.24	0.20	0	5.03	7.08	0.20	9,542	125	931.03
	PGD	0.20	1.69	0.74	12.64	15.23	1.32	4,997	142	4749.08
MobileNet	Test	0.05	1.57	4.81	0	0	0.21	694	37	0.61
	CW	0.19	0.02	0	1.77	1.62	0.14	172	13	0.83
	PGD	0.51	0.36	0	9.71	10.39	0.16	299	16	13.56

two adversarial attack algorithms, Carlini/Wagner (CW) [8] and Project Gradient Descent (PGD) [35]. CW is optimization-based, and it generates AE according to certain optimization objectives. PGD is loss function-based, and it adds perturbations on images which are guided by gradients of the victim DNN. We truncate the adversarial perturbations within $[-0.3, 0.3]$. Perturbations added on AEs are different from white noise, as shown in Fig. 8. AEs are generated using the training data, and all algorithms attacking

Table 8: Transformations for mutating images.

Type	Operator	Remark
Pixel-Level	contrast, brightness	Robustness
Affine	translation, scaling, rotation	Shape bias
Texture-Level	blurring, stylizing	Texture bias

the three models reach over 98% success rates. That is, more than $N \times 0.98$ (N is the size of training data) AEs can trigger erroneous behaviors. We also find that the incorrect predictions uniformly distribute across all classes. To benchmark criteria’s capability of revealing AEs, we check if a criterion can notably respond to AEs; that is, our **ground truth** in Table 7 specifies that a criterion should achieve higher coverage on CW/PGD compared to using test data.

Similar with the previous settings, we first calculate the coverage using training data and then record the increased coverage of test data and AEs. The results are presented in Table 7. NCS, TKNC, TKNP and CC have higher coverage for the test data than AEs. We interpret that these criteria are not correlated with the fault-revealing capability of a test suite. Note that AEs are generated using training data and the perturbations are truncated within a small range. We thus interpret that AEs are regarded as similar with the training data by these criteria. Furthermore, given that $\times 1$ scheme in Table 4 increases comparable coverage with the test data, these criteria seem more sensitive to white noise instead of adversarial perturbations despite that the white noise lies in an even smaller range $[-0.1, 0.1]$.

KMNC has nearly no response to AEs, but NBC and SNAC respond notably towards AEs. The reason is straightforward: we find that AEs primarily lead to out-of-range neuron outputs. NLC generally measures how divergent a layer output is and responds to the density change of layer outputs. Therefore, the out-of-range neuron outputs, which either induce a higher variance or introduce a low-density layer output, can be captured by NLC. NC responds more to AEs when compared with NCS. The key difference between NC and NCS is that NCS operates on the rescaled values, thus it monitors the relative top percent neurons. If all neuron outputs are increased with the same value, there will be no coverage increase.

7.2 Guiding Input Mutation

This section uses existing criteria and NLC as the objective to guide input mutation. This denotes a typical feedback-driven (fuzz) testing setting, where inputs are mutated to maximize the feedback yielded by the criteria. We evaluate the mutated inputs on 1) #triggered faults, 2) naturalness, and 3) diversity of the erroneous behaviors.

**Figure 9: Stylizing and blurring.**

Setting. We use the same image classification models and datasets as in Sec. 7.1. Table 8 lists all mutation methods. Existing efforts mostly mutate images at the pixel level or using affine operators [37, 59]. However, DNNs trained on natural pictures have

Algorithm 1: Fuzzing algorithm.

```

1 Transformation Set:  $T$ ; Fuzzing Seed:  $S$ ;
2 Tested DNN:  $D$ ; Criterion:  $C$ ;  $num \leftarrow 50$ ;
3 while not terminate() do
4    $s = \text{sample}(S)$ ;
5   for  $i \leftarrow 0$  to  $num$  by 1 do
6      $t = \text{sample}(T)$ ;
7      $\hat{s} \leftarrow t(s)$ ;
8     if  $\text{is\_valid}(\hat{s}, s)$  and  $\text{coverage\_inc}(C, D)$  then
9        $S.\text{add}(\hat{s})$ ;
10       $\text{update\_coverage}(C)$ ;
11      break;
12   end
13 end
14 end

```

Table 9: #Faults, naturalness and erroneous behaviors of ResNet trained on ImageNet.

	Rand	NC $T=0$	NCS $T=0.75$	KMNC $K=100$	NBC	SNAC	TKNC $K=10$	TKNP $K=50$	CC $T=1000$	NLC
#Faults	6,488	911	3,309	0	5	8	3,127	7,190	7,902	9,975
#Image	10,000	1,143	4,157	0	6	10	3,967	10,000	10,000	10,000
Rate (%)	64.88	79.70	79.60	0	83.33	80.00	78.83	71.90	79.02	99.75
IS	8.05	7.61	8.05	N/A	1.85	2.62	7.82	7.77	7.13	8.14
FID	131.85	125.31	99.35	N/A	367.84	372.49	99.87	101.08	102.84	98.87
#Class	595	367	672	0	4	7	668	711	708	732
Entropy	0.82	0.92	0.91	0	0.96	0.97	0.90	0.87	0.86	0.88

a *texture-bias* [6, 15], meaning they generate predictions overly depending on an image’s texture. Concerning that operators in Table 8 cannot fully examine DNN behaviors, we prepare texture-level transformations. Studies in the AI community show that training DNNs on stylized images (see Fig. 9) reduces texture-bias [15]. Similarly, blurring, a convolutional operator, smooths texture while keeping object shape in an image. Stylization and blurring are hence used as texture-level transformations.

We launch fuzzing using either prior coverage criteria or NLC according to Alg. 1. *terminate()* returns True when reaching 10K iterations. *is_valid()* is adopted from [54], which deems a mutation as valid if 1) the #changed-pixels is less than $\alpha \times \text{\#pixels}$ or 2) the maximum of changed pixel value is less than $\beta \times 255$. We set α to 0.2 and β to 0.4. As a baseline, we do not check validity and coverage (line 8 in Alg. 1) for random mutation. That is, line 8 in Alg. 1 always yields true for random mutation. We randomly select 1K inputs from the test dataset as the fuzzing seeds.

Faults. The #triggered faults of ResNet trained on ImageNet are presented in Table 9. We also evaluate fuzzing ResNet on trained CIFAR10, a smaller dataset. We note that those results are highly *consistent* with Table 9.

Images mutated under the guidance of NLC (the last column) have the highest error triggering rates compared with random mutation (second column) and other criteria, especially for NBC and SNAC. The fuzzing guided by KMNC even has no output. Recall that these criteria denote a neuron as activated if its output is higher than a threshold or is out-of-range. Since modern DNNs frequently normalize inputs and intermediate neuron outputs, layer outputs tend to concentrate to certain regions (as reflected in Fig. 1). Without fine-grained feedbacks such as gradients, mutated images can hardly flip an unactivated neuron into activated. Nevertheless, we find that the degree of entanglement among neurons can vary w.r.t. mutated inputs. Thus, NLC is very effective to serve the fuzzing guidance, achieving the highest #faults and fault-triggering rates.

TKNP and CC have decent performance; TKNP records the patterns of activated neurons (Sec. 3.2), which, to some extent, can reflect the distribution of layer outputs and entanglement of neurons. CC measures the #regions formed by several neurons, which is correlated with the divergence of DNN outputs.

We also measure how each operator in Table 8 can mutate images and increase coverage. An interesting finding is that texture-level transformations are mostly preferred by fuzzing guided by all criteria, including NLC. Previous criteria primarily use stylizing transformation whereas NLC prefers both blurring and stylizing. This indicates that previous criteria and NLC all explore DNN’s texture-bias. Moreover, since NLC describes the entanglement of neurons, it captures DNN behaviors more comprehensively.

Naturalness. Contemporary testing works have pointed out the importance of preserving naturalness of mutated images [17]. We measure the naturalness of mutated inputs under each criterion; a good criterion should lead to mutations that mostly preserve the naturalness. We use Inception Score (IS) [44] and Fr chet Inception Distance (FID) [21], which are widely used in the AI community to assess the naturalness of images, as the metrics. A higher IS score is better, whereas a lower FID score indicates better naturalness. The evaluation results are also listed in Table 9.

The IS and FID scores of random mutation are regarded as the baseline. Overall, mutated images guided by NLC have the *best performance* regarding both IS and FID scores. We note that mutated images guided by NBC and SNAC manifests relatively low naturalness. Since these two criteria denote a neuron as activated if it has *out-of-range* outputs, its guided mutations incline to largely modify pixel values. We find that the mutated images become less recognizable, e.g., a region in an image gets covered by a black block. Overall, since neurons jointly process features in an input image, mutation with the aim of covering different neuron entanglements are, holistically, “bounded” by features.

Diversity of Erroneous Behaviors. A higher diversity of erroneous behaviors indicates uncovering a practically larger vulnerability surface of DNN models. Overall, a collection of fault-triggering images are regarded as more diverse if they cover more classes. In case that #covered classes is equal, we further use the scaled entropy, $-\frac{1}{|C|} \sum p_c \log p_c$ where p_c is the ratio of incorrect outputs predicted as class c and $|C|$ is the #classes, to assess the diversity; a higher entropy is better. The results are also presented in Table 9. It is seen that fault-triggering images generated by using NLC as the guidance cover the most classes. We thus envision equipping fuzz testing frameworks with NLC to likely identify more and diverse defects from real-world critical DNN systems. Diversity evaluation on CIFAR10 also reports promising and consistent results.

8 RELATED WORK

In addition to testing criteria reviewed in Sec. 3.2, we review the following two aspects in terms of DNN testing.

Testing Oracles. Preparing a validation dataset with labelled data is the traditional way to benchmark DNNs. However, standard dataset, with limited labelled data, can only reflect the hold-out accuracy [37, 41, 49, 58]. Many corner cases (e.g., a snowy traffic scene) can be rarely included. Currently, the SE community primarily uses testing schemes carrying implicit oracles. For example,

metamorphic testing can determine if a DNN model responds consistently to mutated inputs [12, 51, 53, 59]. Similarly, differential testing [37, 51] evaluates if a group of DNN models make consistent predictions when given mutant inputs. Domain-specific oracles for model robustness [52], fairness [13, 60], and interpretability [20, 50] have also been proposed.

Input Mutation. DNN models excel at interpreting real-world data such as images and text. Pixel-level mutations are used to mutate images [37]. However, pixel-level mutations can be inefficient, and extending such byte-level mutations to discrete data like text is obscure. The use of affine modifications [51] such as image rotation, scaling, and shearing has recently been proposed. Some domain-specific transformations are also defined over text or images, e.g., applying foggy filters [13, 33, 49, 51, 56, 59, 60]. Some AI models are also used to change inputs, such as generating synonyms for a masked sentence [19] or synthesizing severe driving scenes [59].

9 CONCLUSION

Inspired by the observations that DNNs are designed to approximate distributions, we propose eight design principles for DNN testing criteria. We design NLC, a testing criterion that satisfies all eight design requirements. NLC describes distributions of single neuron output, neuron relations in a layer, and layer hierarchical relations in a DNN. We show that NLC can facilitate better test input assessment and serve as guidance of fuzz testing.

REFERENCES

- [1] [n.d.]. The official codebase of DeepXplore. <https://github.com/peikexin9/deepxplore>.
- [2] Richard Bellman. 1966. Dynamic programming. *Science* 153, 3731 (1966), 34–37.
- [3] Yoshua Bengio, Aaron Courville, and Pascal Vincent. 2013. Representation learning: A review and new perspectives. *IEEE transactions on pattern analysis and machine intelligence* 35, 8 (2013), 1798–1828.
- [4] Christopher M Bishop et al. 1995. *Neural networks for pattern recognition*. Oxford university press.
- [5] Hans-Dieter Block. 1962. The perceptron: A model for brain functioning. *Reviews of Modern Physics* 34, 1 (1962), 123.
- [6] Wieland Brendel and Matthias Bethge. 2019. Approximating cnns with bag-of-local-features models works surprisingly well on imagenet. *arXiv preprint arXiv:1904.00760* (2019).
- [7] Andrew Brock, Jeff Donahue, and Karen Simonyan. 2018. Large Scale GAN Training for High Fidelity Natural Image Synthesis. In *International Conference on Learning Representations*.
- [8] Nicholas Carlini and David Wagner. 2017. Towards evaluating the robustness of neural networks. In *2017 IEEE Symposium on Security and Privacy (SP)*. IEEE, 39–57.
- [9] Tianqi Chen, Thierry Moreau, Ziheng Jiang, Lianmin Zheng, Eddie Yan, Haichen Shen, Meghan Cowan, Leyuan Wang, Yuwei Hu, Luis Ceze, et al. 2018. {TVM}: An automated end-to-end optimizing compiler for deep learning. In *13th {USENIX} Symposium on Operating Systems Design and Implementation ({OSDI} 18)*. 578–594.
- [10] Jia Deng, Wei Dong, Richard Socher, Li-Jia Li, Kai Li, and Li Fei-Fei. 2009. Imagenet: A large-scale hierarchical image database. In *2009 IEEE conference on computer vision and pattern recognition*. Ieee, 248–255.
- [11] Li Deng. 2012. The mnist database of handwritten digit images for machine learning research [best of the web]. *IEEE Signal Processing Magazine* 29, 6 (2012), 141–142.
- [12] Anurag Dwarakanath, Manish Ahuja, Samarth Sikand, Raghotham M. Rao, R. P. Jagadeesh Chandra Bose, Neville Dubash, and Sanjay Podder. 2018. Identifying Implementation Bugs in Machine Learning Based Image Classifiers Using Metamorphic Testing. In *ISSTA*.
- [13] Cynthia Dwork, Moritz Hardt, Toniann Pitassi, Omer Reingold, and Richard Zemel. 2012. Fairness through awareness. In *Proceedings of the 3rd innovations in theoretical computer science conference*. 214–226.
- [14] Ronen Feldman. 2013. Techniques and applications for sentiment analysis. *Commun. ACM* 56, 4 (2013), 82–89.

- [15] Robert Geirhos, Patricia Rubisch, Claudio Michaelis, Matthias Bethge, Felix A. Wichmann, and Wieland Brendel. 2019. ImageNet-trained CNNs are biased towards texture; increasing shape bias improves accuracy and robustness. In *International Conference on Learning Representations*. <https://openreview.net/forum?id=Bygh9j09KKX>
- [16] Ian Goodfellow, Jean Pouget-Abadie, Mehdi Mirza, Bing Xu, David Warde-Farley, Sherjil Ozair, Aaron Courville, and Yoshua Bengio. 2014. Generative adversarial nets. In *Advances in neural information processing systems*. 2672–2680.
- [17] Fabrice Harel-Canada, Lingxiao Wang, Muhammad Ali Gulzar, Quanquan Gu, and Miryung Kim. 2020. Is neuron coverage a meaningful measure for testing deep neural networks?. In *Proceedings of the 28th ACM Joint Meeting on European Software Engineering Conference and Symposium on the Foundations of Software Engineering*. 851–862.
- [18] Kaiming He, Xiangyu Zhang, Shaoqing Ren, and Jian Sun. 2016. Deep residual learning for image recognition. In *Proceedings of the IEEE conference on computer vision and pattern recognition*. 770–778.
- [19] Pinjia He, Clara Meister, and Zhendong Su. 2020. Structure-invariant testing for machine translation. In *ICSE*.
- [20] Bernease Herman. 2017. The promise and peril of human evaluation for model interpretability. *arXiv preprint arXiv:1711.07414* (2017), 8.
- [21] Martin Heusel, Hubert Ramsauer, Thomas Unterthiner, Bernhard Nessler, and Sepp Hochreiter. 2017. Gans trained by a two time-scale update rule converge to a local nash equilibrium. In *Advances in neural information processing systems*. 6626–6637.
- [22] Sepp Hochreiter and Jürgen Schmidhuber. 1997. Long short-term memory. *Neural computation* 9, 8 (1997), 1735–1780.
- [23] Andrew G Howard, Menglong Zhu, Bo Chen, Dmitry Kalenichenko, Weijun Wang, Tobias Weyand, Marco Andreetto, and Hartwig Adam. 2017. Mobilenets: Efficient convolutional neural networks for mobile vision applications. *arXiv preprint arXiv:1704.04861* (2017).
- [24] Sergey Ioffe and Christian Szegedy. 2015. Batch normalization: Accelerating deep network training by reducing internal covariate shift. In *International conference on machine learning*. PMLR, 448–456.
- [25] Jinhan Kim, Robert Feldt, and Shin Yoo. 2019. Guiding Deep Learning System Testing Using Surprise Adequacy. In *ICSE*.
- [26] Jinhan Kim, Jeongil Ju, Robert Feldt, and Shin Yoo. 2020. Reducing dnn labelling cost using surprise adequacy: An industrial case study for autonomous driving. In *Proceedings of the 28th ACM Joint Meeting on European Software Engineering Conference and Symposium on the Foundations of Software Engineering*. 1466–1476.
- [27] Diederik P Kingma and Max Welling. 2013. Auto-encoding variational bayes. *arXiv preprint arXiv:1312.6114* (2013).
- [28] Alex Krizhevsky, Geoffrey Hinton, et al. 2009. Learning multiple layers of features from tiny images. (2009).
- [29] Hsin-Ying Lee, Hung-Yu Tseng, Jia-Bin Huang, Maneesh Singh, and Ming-Hsuan Yang. 2018. Diverse image-to-image translation via disentangled representations. In *Proceedings of the European conference on computer vision (ECCV)*. 35–51.
- [30] Yu Liu, Fangyin Wei, Jing Shao, Lu Sheng, Junjie Yan, and Xiaogang Wang. 2018. Exploring disentangled feature representation beyond face identification. In *Proceedings of the IEEE Conference on Computer Vision and Pattern Recognition*. 2080–2089.
- [31] Lei Ma, Felix Juefei-Xu, Jiyuan Sun, Chunyang Chen, Ting Su, Fuyuan Zhang, Minhui Xue, Bo Li, Li Li, Yang Liu, et al. [n.d.]. DeepGauge: Comprehensive and multi-granularity testing criteria for gauging the robustness of deep learning systems. In *Proceedings of the 33rd ACM/IEEE International Conference on Automated Software Engineering (ASE 2018)*.
- [32] Lingxiao Ma, Zhiqiang Xie, Zhi Yang, Jilong Xue, Youshan Miao, Wei Cui, Wenxiang Hu, Fan Yang, Lintao Zhang, and Lidong Zhou. 2020. Rammer: Enabling Holistic Deep Learning Compiler Optimizations with rTasks. In *14th {USENIX} Symposium on Operating Systems Design and Implementation ({OSDI} '20)*. 881–897.
- [33] Pingchuan Ma, Shuai Wang, and Jin Liu. 2020. Metamorphic Testing and Certified Mitigation of Fairness Violations in NLP Models. In *IJCAI*. 458–465.
- [34] Andrew Maas, Raymond E Daly, Peter T Pham, Dan Huang, Andrew Y Ng, and Christopher Potts. 2011. Learning word vectors for sentiment analysis. In *Proceedings of the 49th annual meeting of the association for computational linguistics: Human language technologies*. 142–150.
- [35] Aleksander Madry, Aleksandar Makelov, Ludwig Schmidt, Dimitris Tsipras, and Adrian Vladu. 2017. Towards deep learning models resistant to adversarial attacks. *arXiv preprint arXiv:1706.06083* (2017).
- [36] Augustus Odena and Ian Goodfellow. 2018. Tensorfuzz: Debugging neural networks with coverage-guided fuzzing. *arXiv preprint arXiv:1807.10875* (2018).
- [37] Kexin Pei, Yinzi Cao, Junfeng Yang, and Suman Jana. 2017. DeepXplore: Automated Whitebox Testing of Deep Learning Systems. In *Proceedings of the 26th Symposium on Operating Systems Principles (Shanghai, China) (SOSP '17)*. ACM, New York, NY, USA, 1–18. <https://doi.org/10.1145/3132747.3132785>
- [38] Carl Edward Rasmussen et al. 1999. The infinite Gaussian mixture model. In *NIPS*, Vol. 12. Citeseer, 554–560.
- [39] Jie Ren, Mingjie Li, Zexu Liu, and Quanshi Zhang. 2021. Interpreting and Disentangling Feature Components of Various Complexity from DNNs. In *International Conference on Machine Learning*. PMLR, 8971–8981.
- [40] Douglas A Reynolds. 2009. Gaussian mixture models. *Encyclopedia of biometrics* 741 (2009), 659–663.
- [41] Marco Tulio Ribeiro, Tongshuang Wu, Carlos Guestrin, and Sameer Singh. 2020. Beyond Accuracy: Behavioral Testing of NLP Models with CheckList. In *Proceedings of the 58th Annual Meeting of the Association for Computational Linguistics*. Association for Computational Linguistics, Online, 4902–4912. <https://doi.org/10.18653/v1/2020.acl-main.442>
- [42] Frank Rosenblatt. 1958. The perceptron: a probabilistic model for information storage and organization in the brain. *Psychological review* 65, 6 (1958), 386.
- [43] Nadav Rotem, Jordan Fix, Saleem Abdulrasool, Garret Catron, Summer Deng, Roman Dzhabarov, Nick Gibson, James Hegeman, Meghan Lele, Roman Levenstein, et al. 2018. Glow: Graph lowering compiler techniques for neural networks. *arXiv preprint arXiv:1805.00907* (2018).
- [44] Tim Salimans, Ian Goodfellow, Wojciech Zaremba, Vicki Cheung, Alec Radford, and Xi Chen. 2016. Improved techniques for training gans. *Advances in neural information processing systems* 29 (2016), 2234–2242.
- [45] Jürgen Schmidhuber. 2015. Deep learning in neural networks: An overview. *Neural networks* 61 (2015), 85–117.
- [46] Karen Simonyan and Andrew Zisserman. 2014. Very deep convolutional networks for large-scale image recognition. *arXiv preprint arXiv:1409.1556* (2014).
- [47] Jorge Sola and Joaquin Sevilla. 1997. Importance of input data normalization for the application of neural networks to complex industrial problems. *IEEE Transactions on nuclear science* 44, 3 (1997), 1464–1468.
- [48] Youcheng Sun, Xiaowei Huang, Daniel Kroening, James Sharp, Matthew Hill, and Rob Ashmore. 2018. Testing deep neural networks. *arXiv preprint arXiv:1803.04792* (2018).
- [49] Zeyu Sun, Jie M Zhang, Mark Harman, Mike Papadakis, and Lu Zhang. 2020. Automatic testing and improvement of machine translation. In *Proceedings of the ACM/IEEE 42nd International Conference on Software Engineering*. 974–985.
- [50] Yongqiang Tian, Shiqing Ma, Ming Wen, Yepang Liu, Shing-Chi Cheung, and Xiangyu Zhang. 2021. To what extent do DNN-based image classification models make unreliable inferences? *Empirical Software Engineering* 26, 5 (2021), 1–40.
- [51] Yuchi Tian, Kexin Pei, Suman Jana, and Baishakhi Ray. 2018. DeepTest: Automated Testing of Deep-neural-network-driven Autonomous Cars (ICSE '18).
- [52] Vincent Tjeng, Kai Xiao, and Russ Tedrake. 2017. Evaluating robustness of neural networks with mixed integer programming. *arXiv preprint arXiv:1711.07356* (2017).
- [53] Shuai Wang and Zhendong Su. 2020. Metamorphic Object Insertion for Testing Object Detection Systems. In *ASE*.
- [54] Xiaofei Xie, Lei Ma, Felix Juefei-Xu, Hongxu Chen, Minhui Xue, Bo Li, Yang Liu, Jianjun Zhao, Jianxiong Yin, and Simon See. 2018. Coverage-guided fuzzing for deep neural networks. *arXiv preprint arXiv:1809.01266* (2018).
- [55] Guorong Xuan, Wei Zhang, and Peiqi Chai. 2001. EM algorithms of Gaussian mixture model and hidden Markov model. In *Proceedings 2001 International Conference on Image Processing (Cat. No. 01CH37205)*, Vol. 1. IEEE, 145–148.
- [56] Yuanyuan Yuan, Shuai Wang, Mingyue Jiang, and Tsong Yueh Chen. 2021. Perception Matters: Detecting Perception Failures of VQA Models Using Metamorphic Testing. In *Proceedings of the IEEE/CVF Conference on Computer Vision and Pattern Recognition*. 16908–16917.
- [57] Matthew D Zeiler and Rob Fergus. 2014. Visualizing and understanding convolutional networks. In *European conference on computer vision*. Springer, 818–833.
- [58] Jie M Zhang, Mark Harman, Lei Ma, and Yang Liu. 2020. Machine learning testing: Survey, landscapes and horizons. *IEEE Transactions on Software Engineering* (2020).
- [59] Mengshi Zhang, Yuqun Zhang, Lingming Zhang, Cong Liu, and Sarfraz Khurshid. 2018. DeepRoad: GAN-based Metamorphic Testing and Input Validation Framework for Autonomous Driving Systems. In *ASE*.
- [60] Indre Zliobaite. 2017. Fairness-aware machine learning: a perspective. *arXiv preprint arXiv:1708.00754* (2017).